Impact of atmospheric parameters on the atmospheric Cherenkov technique ⋆

Konrad Bernlöhr

Max-Planck-Institut für Kernphysik
Postfach 103980, 69029 Heidelberg, Germany

Abstract

Atmospheric density profiles as well as several light absorption and scattering processes depend on geographic position and are generally time-variable. Their impact on the atmospheric Cherenkov technique in general (imaging or non-imaging) is investigated. Different density profiles lead to differences in Cherenkov light density of up to 60%. Seasonal variations at mid-latitude sites are of the order of 15–20%. The quest for improved energy calibration of Cherenkov experiments also shows the need for improved transmission calculations, taking all relevant processes into account and using realistic profiles of absorbers. Simulations including the scattering mechanisms also reveal the relevance of Rayleigh and Mie scattering for atmospheric Cherenkov experiments. Refraction and the differences between treating the atmosphere in plane-parallel or spherical geometry are also investigated.

Key words: air shower; Cherenkov light; atmospheric profile; transmission; scattering
PACS: 96.40.Pq; 95.55.Ka

1 Introduction

The atmospheric Cherenkov technique for air-shower detection, in particular the *imaging* atmospheric Cherenkov technique, has become an increasingly mature experimental method of very-high-energy (VHE) γ-ray astronomy [1–4] in recent years. Large effort has gone, for example, into the optimisation of γ-hadron separation, the energy calibration, and the evaluation of spectra

⋆ Based, in part, on work at University of Hamburg and Forschungszentrum Karlsruhe.

of γ-ray sources. Imaging and non-imaging methods play an increasingly important part in measuring the spectrum and composition of cosmic rays, from TeV energies well into the knee region. Among the non-imaging techniques, (former) solar power plants with dedicated Cherenkov equipment [5,6] have begun to achieve unprecedentedly low energy threshold for ground-based γ-ray detectors. The technique of imaging Cherenkov telescopes is also evolving, with several stereoscopic arrays of ten-meter class telescopes now under development [7,8], even larger single telescopes [9], and some hope for further progress in photon detection techniques.

One very important common aspect in all the variants of the atmospheric Cherenkov technique is the atmosphere itself, as the target medium for the VHE cosmic particles, as the emitter of Cherenkov photons, and as the transport medium for those photons.

The present paper tries to further our understanding of several important atmospheric parameters, mainly by extensive numerical simulations. Among the parameters investigated are the vertical profile of the atmosphere, the transmission and scattering of Cherenkov light, the importance of spherical versus plane-parallel geometry in shower simulations (or its insignificance, depending on zenith angle), and the refraction of Cherenkov light. Since available tools were not really adequate for most of the questions involved, the Cherenkov part of the CORSIKA [10] air shower simulation program has been substantially extended and a flexible and very detailed simulation procedure for imaging Cherenkov telescopes developed (although the later is of less relevance for the present paper).

The major goal of this study is to be of practical usefulness for the experimentalist.

2 Atmospheric profiles

For the detection of air showers by particle detectors, a pressure correction is usually sufficient to account for different atmospheric density profiles. For the atmospheric Cherenkov technique the situation is more complex since the shower is not only sampled at one altitude but light is collected from all altitudes. In addition to different longitudinal shower development for different atmospheric density profiles, the atmospheric Cherenkov technique is also sensitive to the index of refraction n. Both the amount of Cherenkov light emitted and its emission angle are affected by the index of refraction at each altitude.

The number of Cherenkov photons emitted per unit path length (in the wave-

length range λ_1 to λ_2) is described by the well-known equation

$$\frac{dN}{dx} = 2\pi\alpha z^2 \int_{\lambda_1}^{\lambda_2} \Big(1 - \frac{1}{(\beta n(\lambda))^2}\Big) \frac{1}{\lambda^2} d\lambda, \tag{1}$$

with α being the fine structure constant ($\approx$1/137), z being the charge number, and $\beta = v/c$. Particles with $\beta < 1/n(\lambda)$ cannot emit Cherenkov light at wavelength λ. At visible wavelengths this results in an energy threshold of more than 20 MeV (35 MeV) for electrons or positrons and about 4.5 GeV (8 GeV) for muons at sea level (at 10 km altitude), respectively. The amount of light emitted by particles above threshold depends on the index of refraction. The opening angle θ_c of the Cherenkov light cone above threshold also depends on n:

$$\cos\theta_c = 1/n\beta \tag{2}$$

which in the limit $\beta = 1$ and for $(n-1) \ll 1$ corresponds to

$$\theta_c \approx \sqrt{2(n-1)} \quad \text{radians.} \tag{3}$$

Different atmospheric density profiles, generally, result in different indices of refraction near shower maximum and, thus, in different amounts of Cherenkov light emitted. Most of the light arriving in the inner region of fairly flat light density (of about 120 m radius at 2000 m altitude) is emitted near and after the shower maximum and is particularly affected by the longitudinal shower development as compared to the total amount of Cherenkov light.

Since $n(\lambda) - 1$ changes by only 5% over the wavelength range 300–600 nm, the range typically covered by photomultipliers, air-shower Cherenkov simulations are usually simplified by assuming a wavelength-independent index of refraction n, obtained at an effective wavelength. Another frequent simplification is to assume that $n - 1$ is proportional to air density but, strictly, n is a more complex function of pressure, temperature, and water vapour content. For the present work, the wavelength independence is also assumed but the dependence on water vapour content etc. is taken into account.

For the purpose of this study the CORSIKA shower simulation program [10] has been adapted to read tables of atmospheric profiles, including density and index of refraction, and suitably interpolate between tabulated values. For the electromagnetic part of the shower development, based on EGS [11], several layers of exponential density profile are used in CORSIKA. Fitting of the corresponding parameters to tabulated vertical profiles can now be done at program start-up. The Cherenkov part of CORSIKA, originally based on

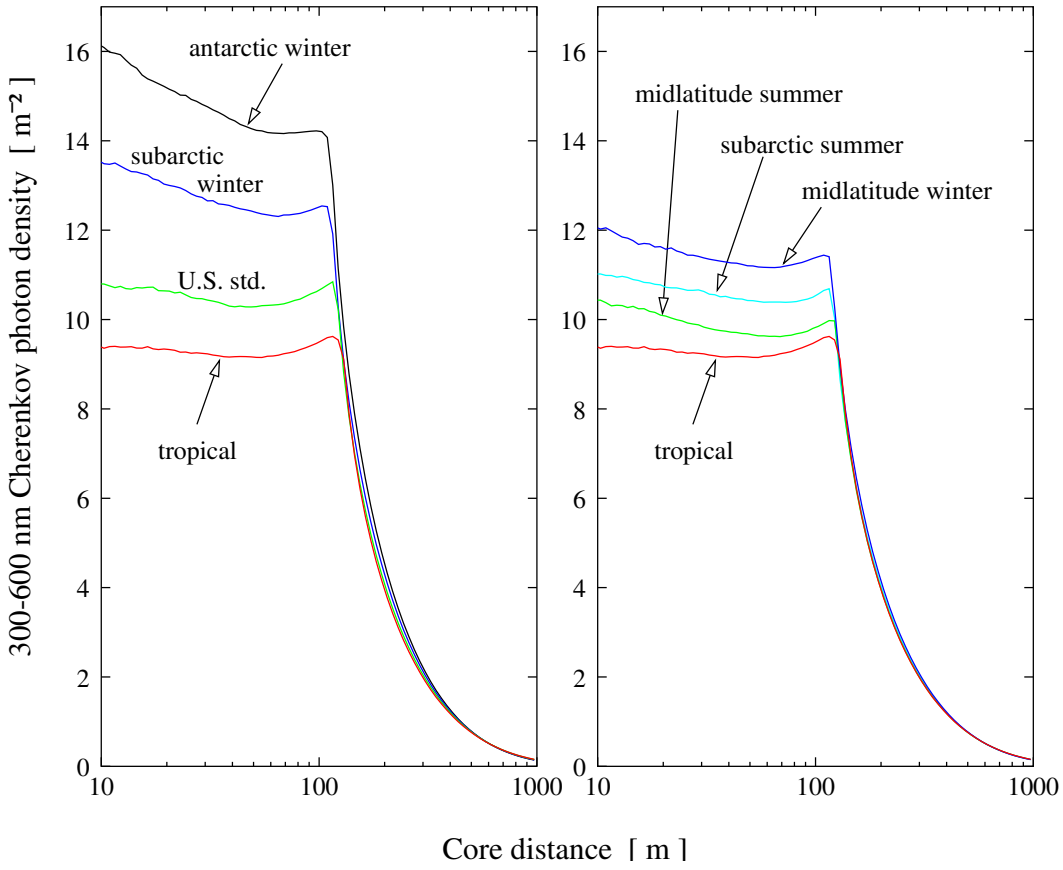

Fig. 1. Average lateral distributions of Cherenkov light photons in the wavelength range 300–600 nm for vertical 100 GeV gamma-ray showers in CORSIKA 5.71 simulations with different atmospheric profiles (2000 showers simulated for each profile). Absorption of Cherenkov light is taken into account (see section 3). Observation altitude is 2200 m above sea level.

work of M. Rozanska, S. Martinez, and F. Arqueros, has been rewritten to account for tabulated indices of refraction and for atmospheric refraction and includes an interface to arbitrary systems of telescopes or other Cherenkov light detectors.

Seven atmospheric tables have been used for this work. Six tables were obtained from the MODTRAN [12] program for atmospheric transmission and radiance calculations (tropical, mid-latitude summer and winter, subarctic summer and winter, and U.S. standard atmosphere 1976). An antarctic winter profile was constructed from radiosonde measurements above the Amundsen-Scott (south pole, 2800 m altitude) and Neumayer (latitude 70° S, near sea level) stations.

Figure 1 shows the quite significant impact of the various atmospheric profiles on the lateral density of Cherenkov light in 100 GeV gamma-ray showers observed at an altitude of 2200 m (the impact being similar for any altitude far beyond shower maximum). The same atmospheric light transmission model

is used in all cases (see section 3). The energy of 100 GeV has been chosen here because it will be a rather typical energy for the next generation of atmospheric Cherenkov experiments and because enough showers can easily be simulated such that shower fluctuations cancel out to a negligible level.

A 60% higher light density near the shower axis is obtained for the antarctic winter as compared to the tropical profile. At moderate latitudes a seasonal effect of 15–20% is apparent and should be included in energy calibrations of IACT installations. Air-shower Cherenkov simulations used for the energy calibration of various experiments have to date mainly used the U.S. Standard Atmosphere 1976 [13] profile. Inappropriate atmospheric models could lead to systematic errors in absolute flux calibrations of the Crab nebula – the de-facto *standard* VHE γ-ray source.

Flux calibrations relative to the (not very accurately known) flux of cosmic rays would be less subject to assumed atmospheric profiles. These relative flux calibrations are most useful for comparison between different experiments but require that the same cosmic-ray flux and composition are assumed. The relative method also depends on applied hadronic interaction models which are still less accurate than electromagnetic shower codes even at energies where accelerator data are available. Note also that, among absolute calibration methods for Cherenkov telescopes, both calibration with a reference light source and with muon rings require detailed knowledge of the spectral response curve since neither the light source nor the muon rings have the same spectrum as the Cherenkov light from near the shower maximum. To a lesser extent this is also true for the relative method because hadron showers with a deeper shower maximum and some light from penetrating muons have, on average, less short-wavelength extinction than gamma showers.

The atmospheric profile is not only important for the average light density at small core distances but also for the radial fall-off. At multi-TeV energies, this radial fall-off is useful as a means to discriminate between hadron and gamma-ray initiated showers and to estimate the cosmic-ray mass composition. Simulations with inappropriate atmospheric profiles could lead to systematics in both cases.

The reasons for the different light profiles are illustrated to some extent by Figure 2, showing the average longitudinal development of showers for four profiles. For profiles with lower temperatures in the lower stratosphere and troposphere the maximum of Cherenkov emission is shifted downwards – to regions of higher density, i.e. higher index of refraction and thus higher Cherenkov efficiency – with respect to profiles with higher temperatures. It should be noted that the atmospheric thickness corresponding to the height of maximum of all Cherenkov emission remains largely unaffected (not more than 5 g/cm^2), but the thickness of the maximum of emission into the inner 50 m

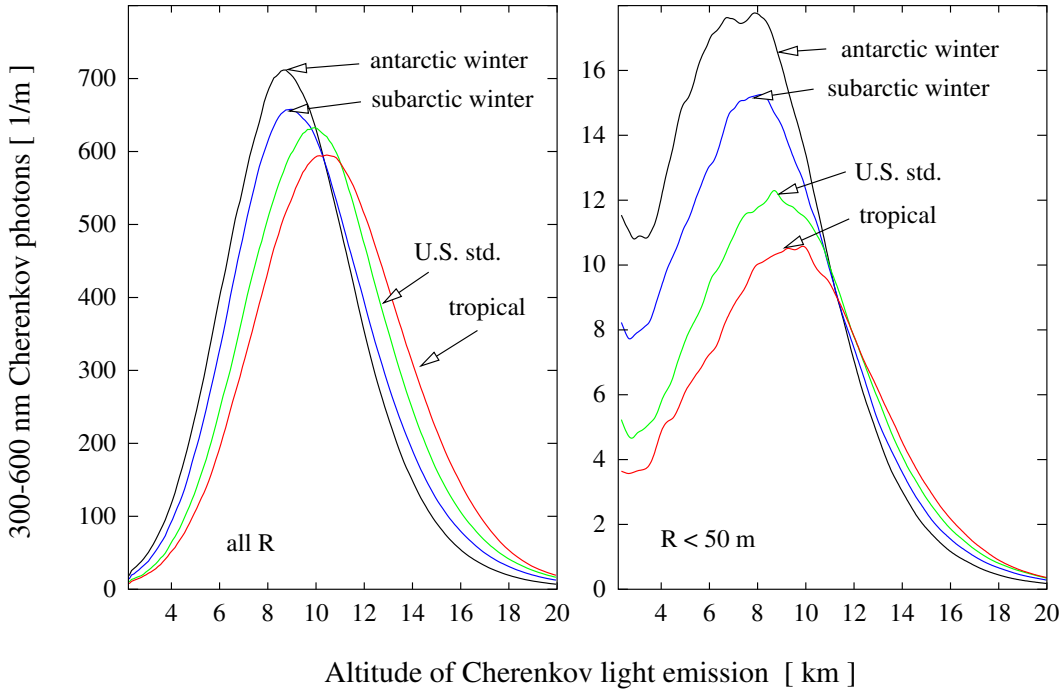

Fig. 2. Average Cherenkov light emission along the shower axis for vertical 100 GeV gamma-rays with different atmospheric profiles. Left: All emitted photons. Right: Photons which would arrive within 50 m from the core at the observation level of 2200 m. No absorption is applied here.

is increasing substantially from the tropical to the antarctic winter profile (by about 30 g/cm^2).

The amount of Cherenkov light within 500 m from the core is roughly proportional to $(n-1)$ at the shower maximum, with about 15% difference between tropical and antarctic winter. If light arriving very far from the shower core is included, the differences are even smaller. Near the core, however, differences are large (see Figure 1) which is due to several effects:

- The amount of Cherenkov emission is roughly proportional to $(n-1)$ at median altitude $h_{\rm med}$ of Cherenkov emission (or at maximum, as before).
- With increasing $(n_{\rm med}-1)$ at $h_{\rm med}$ the Cherenkov cone opening angle is increased and the light is spread over a larger area – decreasing the central light density.
- With decreasing $h_{\rm med}$ the distance between emission maximum and observer is decreased – increasing the central light density.
- For Cherenkov light near the core, the median height of emission $h^{\star}_{\rm med}$ is typically 1000–1500 m below that of all Cherenkov light ($h_{\rm med}$), which emphasises the geometrical factor even more.

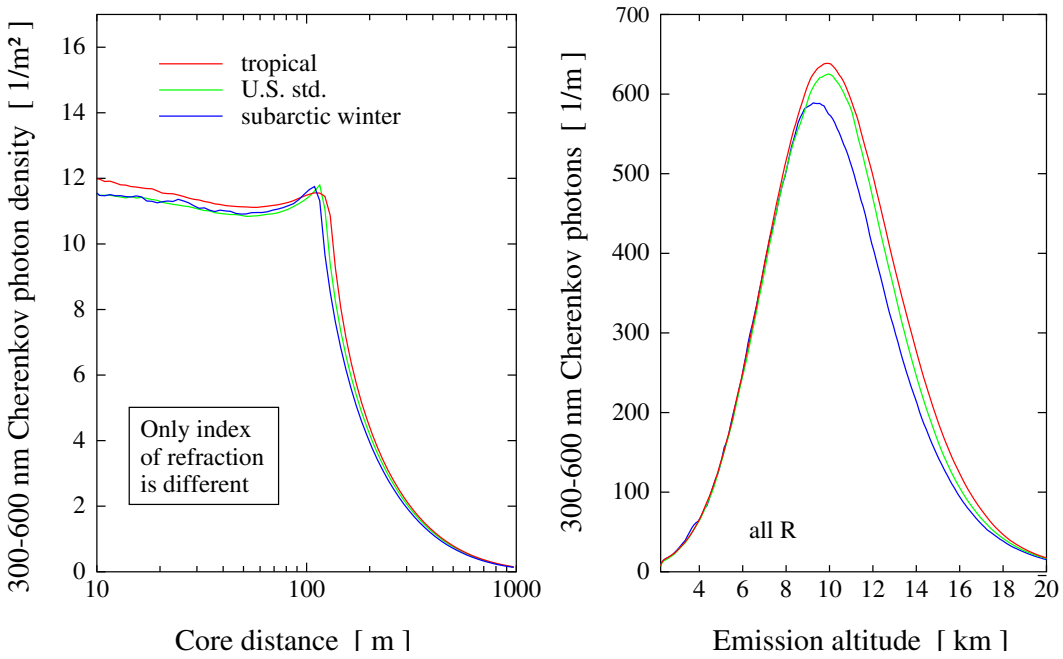

Fig. 3. Cherenkov light profiles when only the index of refraction is taken from different atmospheric profiles but shower development is in all cases simulated with U.S. standard atmosphere. Left: Lateral density of Cherenkov photons (as in Figure 1). Right: Longitudinal profile of Cherenkov emission (as in the left panel of Figure 2).

Qualitatively, the central light density ρ_c for vertical showers follows

$$\rho_c \propto \frac{n_{med} - 1}{(n_{med} - 1)\,(h^\star_{med} - h_{obs})^2} = (h^\star_{med} - h_{obs})^{-2} \qquad (4)$$

where h_{obs} is the observation level altitude. The numerator accounts for the Cherenkov efficiency, the denominator for the area of the light pool. The index of refraction cancels out in this approximation, leaving the distance between $h^\star_{med}$ and h_{obs} as the dominating factor. Since for increasing primary energy h_{med} approaches the observation altitude, the geometrical factor will be increasingly important.

In simulations, it is possible to separate the effects of the atmospheric profiles on shower development and on Cherenkov emission. In Figure 3 the shower development is treated with the CORSIKA built-in U.S. standard atmosphere approximation but the index of refraction is taken from different atmospheric profiles. Since the impact of the different distances between observation level and median emission altitude is not present in this case, any differences in lateral light density are much smaller. The position and shape of the rim of the 'light pool' 100-120 m from the core are the most obvious differences remaining, which are due to different Cherenkov cone opening angles in the lower stratosphere.

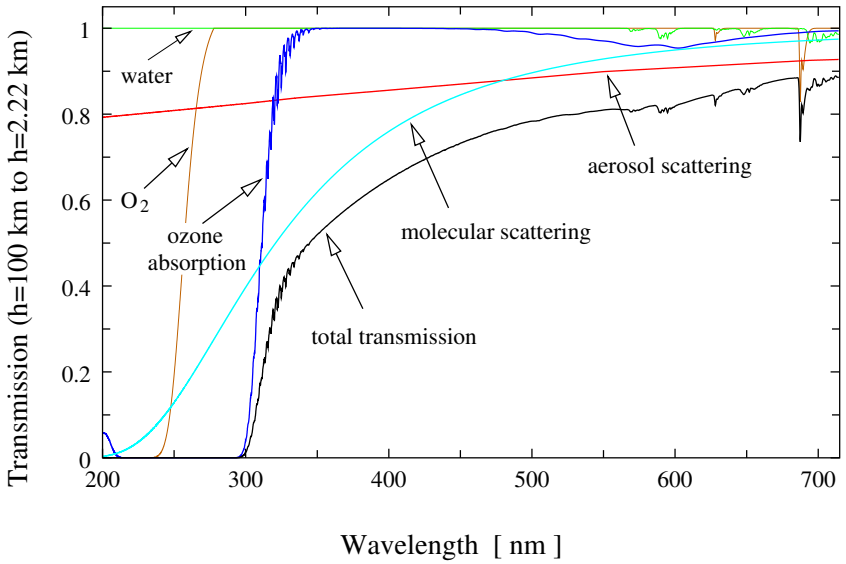

Fig. 4. Direct transmission of light from space (here 100 km altitude) along a vertical path to an altitude of 2.2 km, as calculated with MODTRAN. The impact of the most important absorbers and scatterers is shown.

3 Transmission of Cherenkov light

The atmospheric extinction of light is another source of concern for the energy calibration of atmospheric Cherenkov experiments and to some extent also for the image parameters of telescopes. There are several sources of extinction: absorption bands of several molecules, molecular (Rayleigh) scattering as well as aerosol (Mie) scattering and absorption. For a detailed introduction see for example [14]. The relevance of the various absorbers or scatterers at different wavelengths is illustrated in Figure 4.

At wavelengths below 340 nm ozone (O_3) is a very important absorber – not only in the ozone layer but even near ground. Relevant absorption bands are the Hartley bands in the 200-300 nm range and the Huggins bands extending to 340 nm. Near 600 nm there are the weak Chappuis bands. Normal oxygen (O_2) can be disassociated by light below 242 nm leading to the Hertzberg continuum. In addition, there is the Hertzberg band at 260 nm. The O_2 absorption is of no concern to most Cherenkov experiments – typically using photomultipliers (PMs) with borosilicate glass windows which are insensitive below 290 nm – and is in fact frequently neglected. However, O_2 absorption is a limiting factor for UV observations. Other molecules are of little relevance in the near-UV and visible range.

Most Cherenkov light in the PM sensitivity range is actually lost by molecular scattering. Although some of the light may also be scattered into the viewing angle, such scattered light is generally not important and scattering can be

considered like an absorption process. The same argument applies to aerosols where both scattering and absorption play a role. The relevance of scattered light is discussed in Section 4.

While molecular scattering and O_2 absorption are easily predictable and almost constant at any site, both aerosols and ozone are site-dependent and variable. Aerosols are mainly limited to the *boundary layer* of typically 1–2.5 km thickness above the surrounding terrain where the diurnal variation and the dependence on ground material and wind speed is largest. In the boundary layer, the heating of the ground by solar radiation leads to turbulence and rapid vertical exchange of air and dust. Not just near ground but even in the stratosphere the aerosols play a role – including meteoric and volcanic dust. Ozone also shows diurnal and seasonal variations.

The total extinction of star light is easily measured (and a routine procedure at optical observatories), by fitting the function

$$\ln I(\lambda) = \ln I_0(\lambda) \; - \tau_1(\lambda) \sec z \tag{5}$$

to several observations of a reference star (here in the plane-parallel atmosphere approximation). In this equation I is the measured intensity, I_0 the true intensity, τ_1 the optical depth per unit airmass and $\sec z$ the secant of the zenith angle. For the procedure one or several sources are measured at widely different zenith angles, allowing to fit I_0 and τ_1. This procedure, however, cannot disentangle the vertical structure of absorbers. Different assumptions on this structure easily lead to differences of 5–10% in the amount of Cherenkov light, even at mountain altitude. At sea-level, even differences of up to 30% between different calculations can be traced back to different assumptions on the extinction.

One example of a bad assumption is to take the density of aerosols as proportional to air density. One such example is illustrated in Figure 5. The aerosol-air proportionality assumption leads to an over-estimate (by 4–8%) of Cherenkov light even if the measured star-light extinction at the actual (mountain) altitude is taken into account. The reason for that is that the Cherenkov light is produced, say, halfway down in the atmosphere, implying 50% of the star-light extinction under the assumption, but actually some 80–90% of the aerosol extinction happens below the average Cherenkov production altitude. The aerosol-density proportionality assumption together with the extrapolation of mountain-altitude extinction measurements down to sea level, for example, leads to a severe over-estimate of Cherenkov light intensity at sea level.

A much more realistic model of aerosol vertical structure, aerosol properties plus all the relevant molecular absorption and scattering is included in

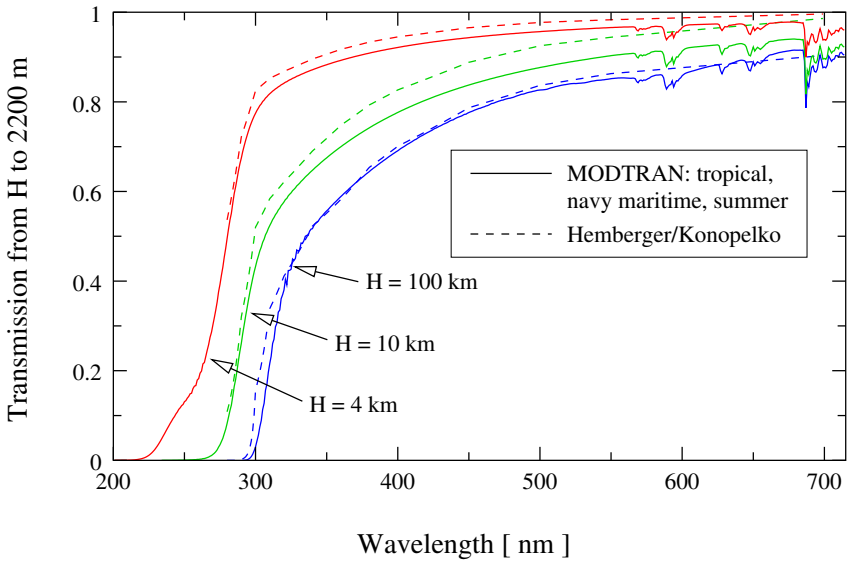

Fig. 5. Comparison of atmospheric transmission as calculated with MODTRAN (using the tropical profile and navy maritime summer haze model) and in a transmission model with aerosol absorption proportional to atmospheric density [15,16]. Note that although both transmission models have almost the same transmission for stellar light, the transmission from typical Cherenkov emission altitudes differs significantly.

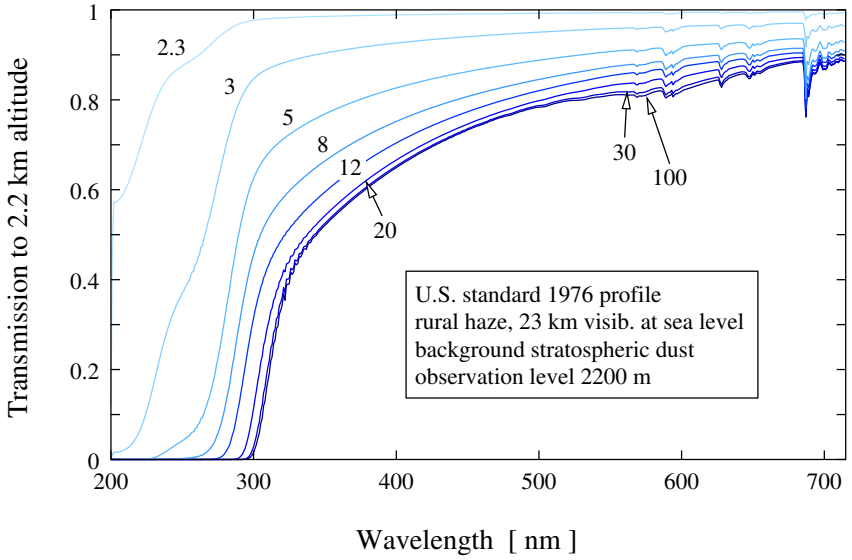

Fig. 6. Direct transmission for light along vertical paths from different altitudes (in km), as noted in the figure, to an observation level of 2200 m. Transmission was calculated with MODTRAN for U.S. standard atmospheric profile, rural haze with 23 km sea level horizontal visibility, and background stratospheric dust.

the MODTRAN [12] program. MODTRAN has been used for the extinction models used in this paper. Unless otherwise noted, a U.S. standard profile with rural haze model of 23 km sea-level horizontal visibility has been used. Transmission curves obtained with this model are shown in Figure 6.

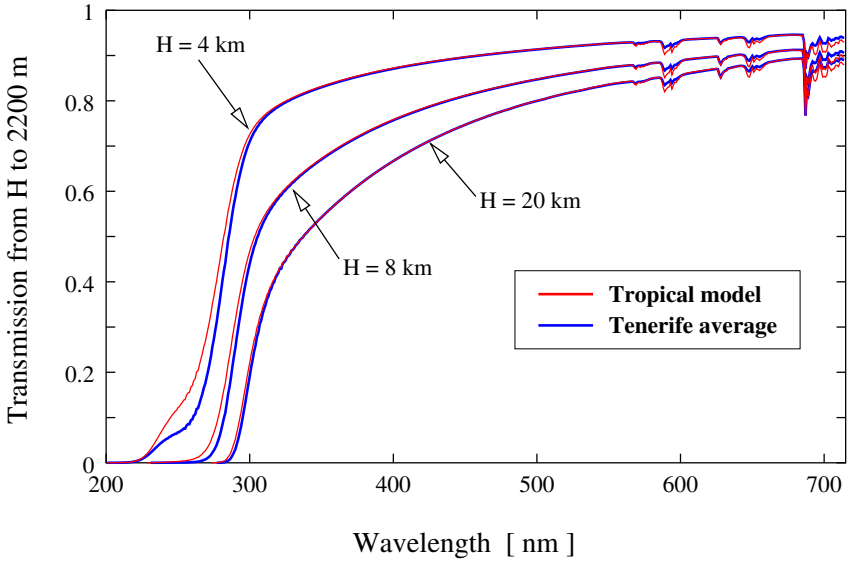

Fig. 7. Impact of the 1.5–2 fold higher ozone content near ground measured [17] with radiosondes from Tenerife, Canary Islands, as compared to the tropical profile. Transmissions calculated with MODTRAN. For the Tenerife model the all-year average data was used. Above the altitude reached by radiosondes (about 32 km), the tropical profile is used. The same maritime haze model is used in both cases.

In the case of the observatory on La Palma (operated by the IAC), the tropical profile and navy maritime haze model – with quite little aerosol extinction – is in excellent agreement with measured extinction curves as well as with the long-term average V band extinction, as provided by the Isacc Newton group on La Palma and the Royal Greenwich Observatory, Cambridge. Temperature and pressure profiles of the MODTRAN tropical profile are also in quite good agreement with radiosonde measurements from the nearby Tenerife island [17]. Tropospheric ozone measurements (with the same radiosondes), however, exceed the MODTRAN model by a factor of 1.5–2. In Figure 7 the transmission curves obtained with the built-in tropical profile and with the profile taken from the radiosonde measurements are compared. For Cherenkov measurements with borosilicate window PMs the differences are insignificant but for UV observations they are important.

As a further atmospheric variable the impact of volcanic dust was studied. The 1991 Pinatubo eruption, for example, led to 30 million tons of stratospheric dust – compared to 1 million tons before the eruption. It is visible in La Palma extinction measurements (obtained with the Carlsberg Meridian Circle and made available by the Royal Greenwich Observatory, Cambridge) for a period of two years. This eruption had a high (5–10%) impact on extinction of stellar light for one and a half years. MODTRAN provides a set of options to enhance the amount of volcanic dust in the calculations. Results for different amounts of dust and different Cherenkov emission altitudes are shown in Figure 8. The volcanic dust extinction is insignificant for altitudes below about 14 km

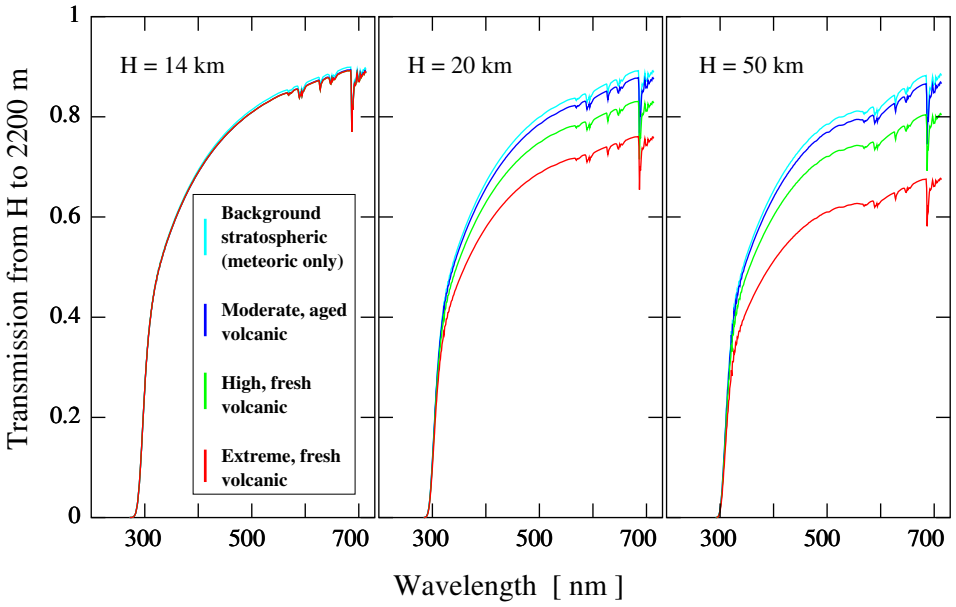

Fig. 8. Atmospheric transmission for different levels of volcanic dust extinction in the stratosphere. The U.S. standard atmospheric profile is used with the rural haze model for tropospheric aerosols and meteoric plus volcanic dust in the stratosphere. The Pinatubo eruption corresponds to activity slightly exceeding the *high* scenario.

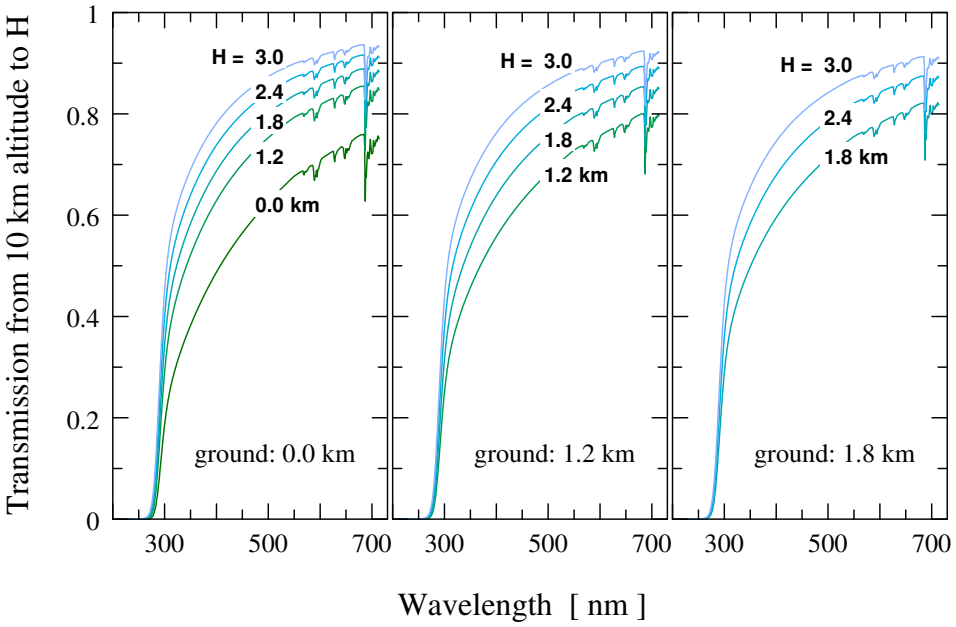

Fig. 9. Atmospheric transmission from 10 km to different observation levels (3.0, 2.4, 1.8, 1.2, and 0.0 km a.s.l.), for three different 'ground' altitudes (left: sea level, middle 1.2 km, right: 1.8 km) as the base of the boundary layer. MODTRAN calculations with U.S. standard atmosphere and rural haze model.

and as such has little impact on Cherenkov measurements. A calibration of Cherenkov telescopes with stellar light under high volcanic dust conditions could lead to an over-estimate of shower energies and, thus, fluxes.

Some of the forthcoming Cherenkov installations [7,8] will likely be installed at the base of a mountain instead of at the top – due to environmental or infrastructure reasons. It seems appropriate to compare the expected atmospheric transmission for sites at different altitudes. Since the aerosol absorption is strongest in the boundary layer, the altitude of the surroundings (on a scale of the order of hundred kilometers and more) is also relevant. If the 'base' of the mountain is still above the boundary layer, the reduced altitude should not affect the transmission very much. If the base is already at the bottom of the boundary layer, even a move from 2.4 km to 1.8 km altitude results in 10% less Cherenkov light (Figure 9, as deduced with the MODTRAN rural haze model). These calculations still assume clear nights while in practice the base of the mountain may be more frequently under a cloud layer or affected by ground fog than the top. This, of course, can only be resolved by a long-term site comparison.

4 Scattering of light

In the preceding discussion, all molecular and aerosol scattering of Cherenkov light is treated as an absorption process. This assumption was apparently used in any atmospheric Cherenkov simulations so far. However, estimates of the impact of scattered Cherenkov light were taken into account for the fluorescence technique [18]. In this section quantitative results of full Cherenkov simulations with scattered light are presented. [1]

When considering scattered light one has to take the relevant integration time into account. Hardly any scattered light will arrive within or even before the Cherenkov light shower front but most scattered light arrives with quite significant delay due to its detour. For short integration times, small-angle scattering is responsible for most of the scattered light.

Rayleigh scattering (of unpolarised light) is described by the simple normalised *phase function* of scattering angle γ

$$P_{\mathrm{R}}(\gamma) = \frac{3}{16\pi}\frac{2}{2+\delta}\left((1+\delta) + (1-\delta)\cos^2\gamma\right) \tag{6}$$

with δ being the depolarisation factor due to anisotropic molecules ($\delta \approx 0.029$). For aerosol scattering – in principle described by Mie scattering theory – the situation is much more complicated and depends on size distribution, composition, and shapes of aerosol particles. In all practical cases, aerosol

[1] Since fluorescence light is not available with CORSIKA yet, these simulations could not be applied to the fluorescence technique at this stage.

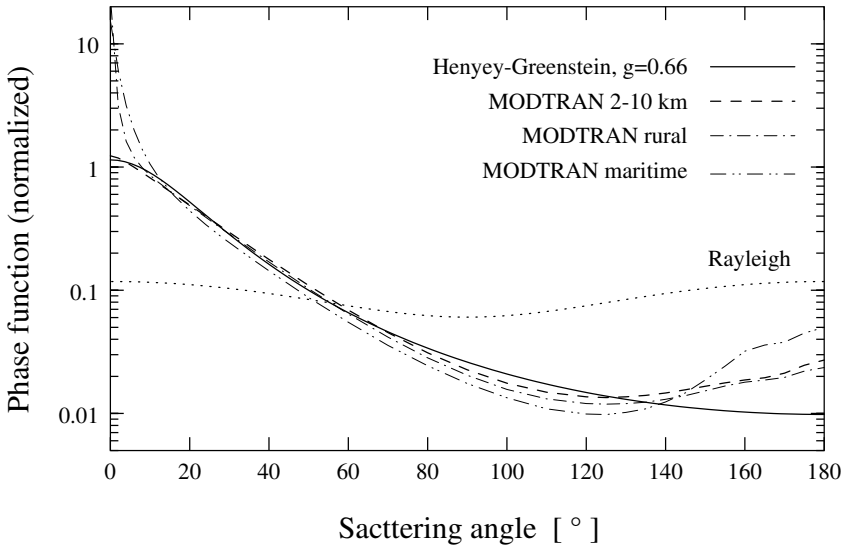

Fig. 10. Phase functions, i.e. relative intensity of scattered light per unit solid angle, for Rayleigh scattering (dotted), the MODTRAN [12] 2–10 km tropospheric aerosol model (dashed) and the Henyey-Greenstein function of $g = 0.66$ (solid line). Also shown: MODTRAN phase functions for rural and maritime 0–2 km boundary layer (thin dot-dashed lines).

scattering is quite asymmetric with a forward peak. Due to its forward peak, aerosol scattering generally dominates over molecular scattering in Cherenkov light measurements with short integration times.

Although Cherenkov light of air showers is partially polarised, the polarisation is ignored in the following because it is only relevant for large-angle scattering. It should also be noted that the amount of aerosol scattering (and to some extent also its phase function) can be highly variable – a fact that is very important for the air shower fluorescence technique where the contamination of the weak fluorescence light by scattered (in addition to direct) Cherenkov light has to be (and usually is) taken into account. In the following, an average amount and phase function for aerosol scattering is assumed which should be more or less typical for a good astronomical site situated well above the boundary layer in which turbulent mixing due to the diurnal temperature cycle is relevant.

Aerosol scattering and absorption coefficients have been calculated with the MODTRAN [12] program. The phase function can be approximated by a Henyey-Greenstein phase function with asymmetry parameter g:

$$P_{\mathrm{HG}}(\gamma) = \frac{1}{4\pi} \frac{(1-g^2)}{(1-2g\cos\gamma+g^2)^{3/2}}. \tag{7}$$

The tropospheric aerosol phase function in MODTRAN has an asymmetry $g = \langle \cos\gamma P_{\mathrm{HG}}(\gamma) \rangle \approx 0.7$ and is in the angle range $0° < \gamma < 140°$ well rep-

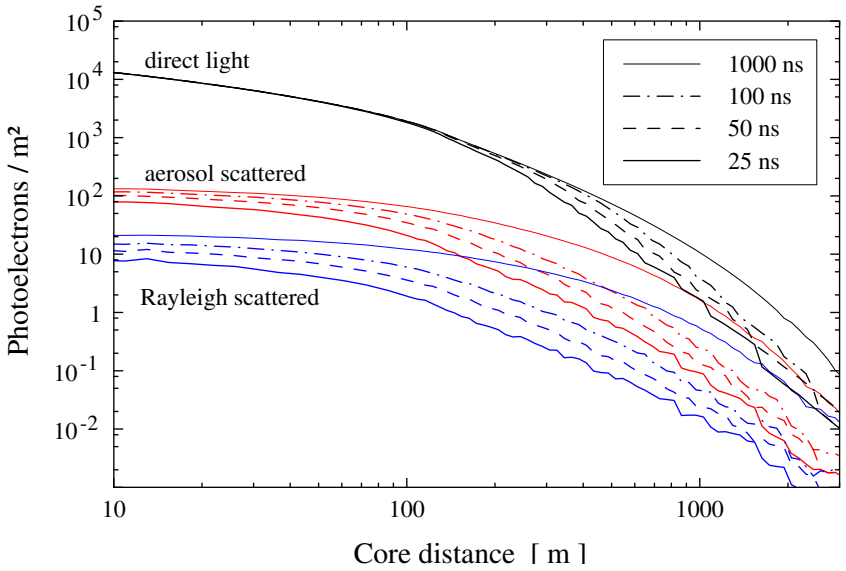

Fig. 11. Lateral density of direct, aerosol scattered, and Rayleigh scattered light in vertical proton showers of 100 TeV primary energy (average of 10 showers) for different integration times. Note that integration intervals at different core distances are shifted approximately such as to maximise the integrated average signal at each distance interval. Mirror reflectivity and PM quantum efficiency curve are applied for the conversion from photons to photo-electrons. A tropical atmospheric profile was used in this case.

resented by a Henyey-Greenstein phase function of $g \approx 0.66$ (see Figure 10). In the following, $g = 0.7$ is used. For the shower simulations with a modified CORSIKA 5.70 program an U.S. standard atmospheric profile was used unless otherwise noted. Atmospheric transmission coefficients (including absorption and scattering on aerosols) were used as calculated with the MODTRAN rural haze model. The scattering algorithm used with CORSIKA includes multiple scatterings although these turned out to be insignificant. An observation level at an altitude of 2200 m is assumed. Since the relevance of scattered light is wavelength dependent, usual observation conditions are simulated by applying the quantum efficiency curve of a photomultiplier (PM) with borosilicate glass window and bi-alkali photocathode and the reflectivity of an aluminised mirror.

The relevance of scattered light integrated over the whole sky is shown in Figure 11 for 100 TeV proton showers. Note that within the central 200 m, 1–3% of the total Cherenkov light is scattered light (for integration times below 100 ns). This fraction is increasing with distance since the lateral distribution of scattered light is flatter than that of the direct light. Within the central kilometer, aerosol scattered light dominates over Rayleigh scattered light. Beyond a few kilometers from the core and for integration times of more than one microsecond, scattered light eventually exceeds the direct light. Note that, for the short integration times, the smaller field of view of non-imaging Cherenkov

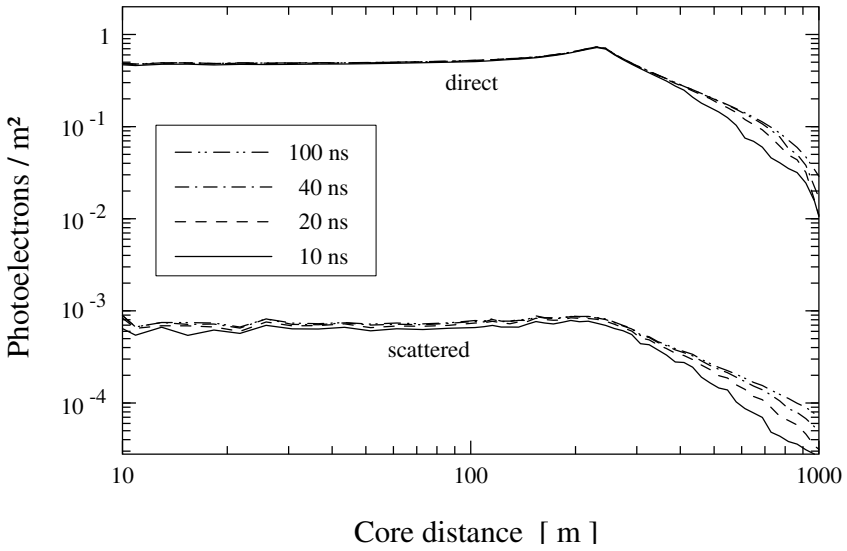

Fig. 12. Lateral distribution of direct and scattered light in 300 GeV γ-showers at a zenith angle of 60° (average of 250 simulated showers). Core distances are given in a plane perpendicular to the shower axis. A 5° diameter field of view has been assumed, and mirror reflectivity and PM quantum efficiency as before.

counters like AIROBICC [19] or even BLANCA [20] will not much reduce the amount of scattered light. Most of the scattered light arriving within a few 10 ns of the direct light is scattered by no more than ten degrees.

In the imaging atmospheric Cherenkov technique the Cherenkov light is integrated over a much smaller field of view and, generally, over a very short time interval (20 ns or even less). In this case the impact of scattered light is even smaller. As a conservative measure of scattered light all light in a 5° diameter field of view of a Cherenkov telescope centered on a gamma source is counted here – although in practice pixels more than 0.5° from the image major axis would generally be below a minimum threshold and not counted. Note that almost all light scattered by less than 2.5° has a delay of less than 10 ns with respect to direct light and short integration times would not significantly suppress scattered light.

In the small field of view of such telescopes the scattered light has approximately the same path length as direct light and the ratio of scattered to direct light approximately scales with the airmass ($1/\cos z$ for a plane-parallel atmosphere). Since experimental groups are more concerned about scattered light in large-zenith-angle observations than near vertical, Figure 12 shows the case for zenith angle $z = 60°$. Even in this case, scattered light is quite marginal (of the order of 10^{-3}).

It should be noted, however, that some aerosol scattering phase function models for the boundary layer (e.g. as in MODTRAN, see Figure 10) have an additional peak in the very forward direction, which is not present in the

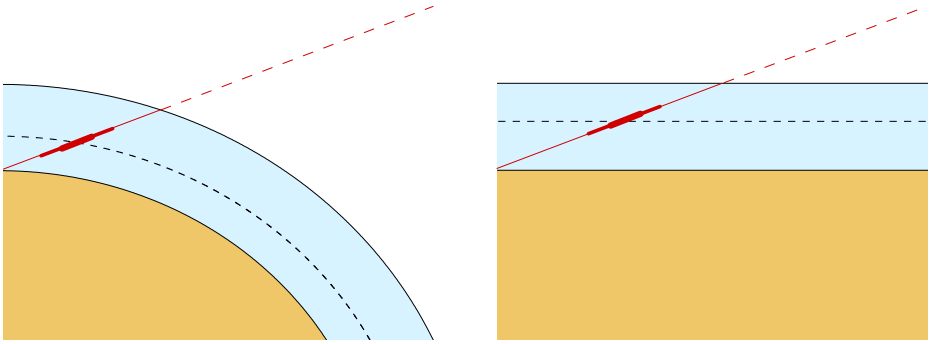

Fig. 13. In the correct spherical description of the atmosphere all slant shower paths have less material to traverse than in the planar description. As a consequence the shower maxima at fixed atmospheric depth are at lower altitudes (dashed lines) in the spherical description.

MODTRAN 2–10 km tropospheric scattering model and not accounted for by the Henyey-Greenstein phase function. Under such circumstances – mainly Cherenkov experiments not far above the surrounding terrain or observing in the presence of thin clouds or fog – small-angle scattering of the Cherenkov light could be up to an order of magnitude more severe. This, for example, is the case in simulations of sea level observations with the MODTRAN rural haze phase function for aerosol scattering in the lower 2 km, where scattered light in the 5° field of view amounts to 1% of direct light at 60° zenith angle. Even at that level, scattered light should not be of major concern.

The impact of thin clouds – which has not been simulated here – should be primarily on the trigger rate. Depending on the cloud altitude, the image *length* parameter could be reduced by losing only light emitted above the layer but the impact of scattered light on image parameters would still be small. Image parameters could rather be affected by the change of night-sky noise – which could either be reduced due to absorption or increased due to scattering of urban light.

5 Planar versus spherical atmosphere

The CORSIKA program is at present using a plane-parallel atmosphere for shower simulations – except for a special, not Cherenkov-enabled, *horizontal* version. The impact of a planar versus a spherical atmosphere, in its qualitative implications, is nevertheless easy to show (see Figure 13). With spherical geometry the shower maximum (at constant atmospheric depth) is at a lower altitude, where the index of refraction is larger and more Cherenkov light is emitted. This geometry effect is only relevant for large zenith angles.

Instead of shower simulations by the Monte Carlo method, an analytical ap-

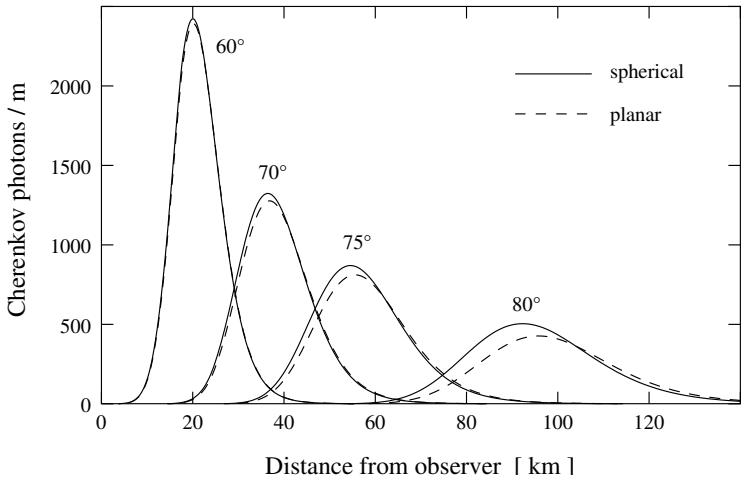

Fig. 14. The average longitudinal Cherenkov emission profile as a function of distance from the observer (Cherenkov photons emitted in the wavelength range 300–600 nm per meter along the shower axis). An analytical approximation is used for different zenith angles (solid lines: spherical geometry, dashed: planar geometry).

proximation of the average Cherenkov emission of gamma showers is used here. It takes the longitudinal shower profile, the Cherenkov emission threshold depending on the index of refraction, and the emission of electrons above threshold into account. This approximation reproduces the longitudinal profile of Cherenkov emission in CORSIKA simulations very well for all model atmospheres. This approximation has been used with both spherical and planar atmospheric geometry to show that the difference is insignificant below 60° zenith angle, and little significant below 70° (see Figure 14). For hadronic showers there is a small additional effect of fewer pions and kaons decaying before the next interaction and, thus, fewer muons with the spherical geometry at very large zenith angles.

6 Refraction

One of the recent achievements in VHE energy γ-astronomy is the fact that TeV γ-ray sources can be located with sub-arcminute accuracy [21]. In addition, observations at large zenith angles are carried out by more and more Cherenkov telescope experiments, either to extend the observation time for a source or the effective area for high-energy showers, or to detect sources only visible at large zenith angles. Refraction of Cherenkov light in the atmosphere is therefore of increasing concern but is usually either neglected entirely or only considered in a qualitative way. The following discussion is based on numerical ray-tracing. The refraction method built into recent CORSIKA versions is based on a fit to such ray-tracing.

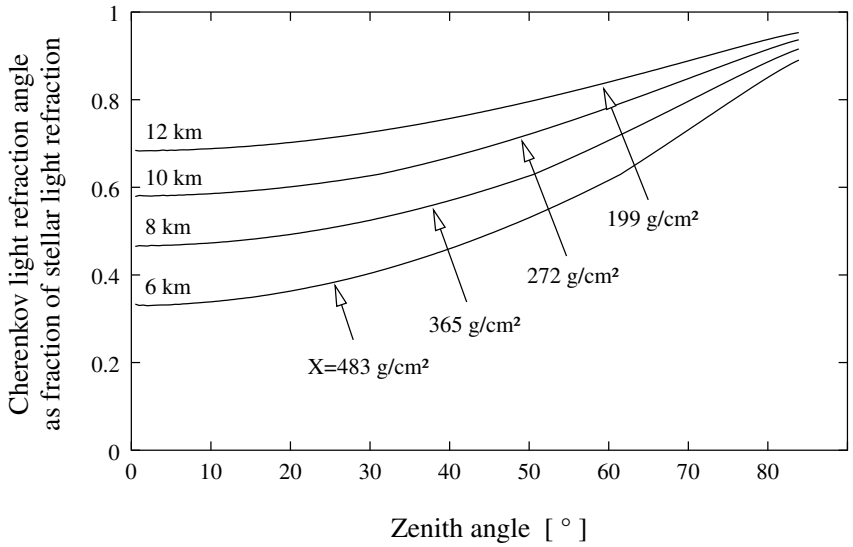

Fig. 15. The refraction angle of Cherenkov light as a function of zenith angle, expressed as a fraction of the corresponding refraction of stellar light. Numerical integrations for U.S. standard atmosphere with spherical geometry and 2200 m observation altitude. Curves shown are for emission at constant atmospheric depth along the shower axis. For vertical showers, the depths of 483, 365, 272, and 199 g cm^{-2} correspond to altitudes of 6, 8, 10, and 12 km, respectively.

For a plane-parallel atmosphere Snell's law of refraction is

$$n(z)\,\sin\theta(z) = \text{const.} \tag{8}$$

with $n(z)$ being the index of refraction at altitude z and $\theta(z)$ being the zenith angle of the ray at this altitude. For a spherical atmosphere

$$n(z)\,(R_\mathrm{E} + z)\,\sin\theta(z) = \text{const.} \tag{9}$$

has to be used instead, with R_E being the earth radius.

The refraction of Cherenkov light emitted in the atmosphere is evidently smaller than that of star light seen from the same direction. Thus, even when using guide stars for tracking of Cherenkov telescopes, a correction for refraction has to be applied to take full advantage of measured shower directions. For γ-showers of 0.1–1 TeV the Cherenkov light is refracted typically 60–50% (70–60%) as much as stellar light up to 40° (near 60°) zenith angle, with less refraction for showers of higher energy (see Figure 15). The different amount of refraction of light from the beginning and the end of the shower, respectively, leads to a change of image length. When an inclined shower is seen from below the axis, it appears slightly shorter, and when seen from above the axis, it appears longer – by a fraction of an arcminute.

Apart from the change in the Cherenkov light direction, refraction also affects

the arrival position and time. The impact on the arrival time is marginal if measured in a plane perpendicular to the shower axis and is well below one nanosecond even at 80° zenith angle. The arrival position in the shower plane is affected by typically 3 meters (18 m) in TeV γ-showers of 60° (75°) zenith angle. Actual changes depend on the height of emission and lead to a small distortion of the lateral shape – the average shift being irrelevant.

7 Conclusions

The impact of a number of atmospheric parameters on the atmospheric Cherenkov technique in general have been presented. It turns out that there are several such parameters which deserve more attention in the experimental analysis. This applies to the imaging technique in VHE γ-ray astronomy and to non-imaging techniques – both in γ-ray and cosmic-ray studies.

The vertical structure of the atmosphere is the most striking of these parameters, with up to 60% difference in Cherenkov light between tropical and polar models and some 15–20% seasonal variation at mid-latitude sites. The appropriate structure could be easily applied in shower simulations for particular sites – while most calculations so far were restricted to US Standard Atmosphere 1976 or similar profiles. Relevant measurements are routine procedure of many meteorological institutions and data are readily available.

Atmospheric extinction of Cherenkov light appears as another area which deserves perhaps more care, as the accuracy of the experiments improves. In particular, the assumption that extinction (scattering and absorption) by aerosols is, like Rayleigh scattering, only a function of traversed atmospheric thickness, is not a very good one. Extrapolation of high-altitude extinction measurements to low-level sites must be avoided. Cherenkov experiments should, at least, apply standard astronomical extinction monitoring procedures – if not already available from co-located optical observatories. In order to reduce energy systematics below ten percent this might, however, not be enough.

Measurement of the aerosol vertical structure is – in contrast to stellar light extinction or to the air density profile – rather difficult. Lidar remote sensing methods, for example, measure primarily the back-scattered amount of light, although lidar methods are available to measure also the extinction profile with a reasonable 10% accuracy. The ratio of back-scattered light to total extinction depends very much on aerosol composition. Even otherwise similar phase functions (see Figure 10) differ easily by a factor of two in the back-scattering regime. As a consequence, some model-dependence will likely remain in transmission calculations but the best available models for a site should be used.

For UV Cherenkov experiments sensitive below 300 nm wavelength, the variations of ozone profiles are an additional area of concern and absorption on oxygen can no longer be ignored.

Scattered Cherenkov light has a rather minor impact for Cherenkov experiments – in contrast to air shower fluorescence experiments. Scattering should, however, be of some concern to wide-angle non-imaging experiments using the Cherenkov light lateral distribution either to discriminate between hadronic and gamma showers or to disentangle the cosmic-ray mass composition.

The assumption of a plane-parallel atmosphere in air shower simulations becomes a problem when going to zenith angles beyond about 75°. These large zenith angles are very important for fluorescence experiments in order to achieve the largest possible effective areas. For Cherenkov γ-ray experiments the increase in effective area, however, will – under most experimental conditions that can be envisaged – be more than counterbalanced by the much worse gamma-hadron discrimination when observing showers from more than 60 km distance. As a consequence, implementation of the proper spherical geometry in shower simulations is of less importance to the Cherenkov than to the fluorescence method.

Atmospheric Cherenkov light refraction – until recently negligible compared to experimental errors – has to be accounted for when locating sources with sub-arcminute accuracy as now possible. For the time being, an approximate correction, e.g. as taken from Figure 15, should generally be sufficient. For more accurate results, enhancements to the CORSIKA code should be available with new CORSIKA versions.

In addition to those atmospheric parameters covered in this paper, there are other, more subtle effects at work. One such example would be the time-variable night-sky background, e.g. due to airglow and scattering of urban illumination – something that should be kept in mind but is probably beyond the scope of what should be or can be accurately modelled in shower simulations.

The geomagnetic field – not covered by this paper – has an additional impact. For present IACT experiments, say at energies of the order of 1 TeV, the main impact is a variation of the Cherenkov light intensity by a few percent between observations parallel to and perpendicular to the field direction. Image parameters are little affected at these energies. For future experiments observing lower energy showers with better angular resolution the geomagnetic field can be expected to be more significant.

Acknowledgements

Radiosonde measurements for Tenerife were kindly provided by the Izana Global Atmospheric Watch (GAW) Observatory. The use of further radiosonde data from the Amundsen-Scott and Neumayer stations is acknowledged, as well as the use of La Palma extinction data provided by the Isaac Newton group on La Palma, Canary Islands, and the Royal Greenwich Observatory, Cambridge. Most of this paper is based on calculations with CORSIKA 5.7 and it is a pleasure to thank its authors, in particular D. Heck, for their support. The MODTRAN 3 v1.5 program was kindly provided by the Phillips Laboratory, Geophysics Directorate, at Hanscom AFB, Massachusetts (USA).

References

[1] T. C. Weekes, Physics Reports 160 (1988) 1.

[2] M. F. Cawley and T. C. Weekes, Experimental Astronomy 6 (1995) 7.

[3] F. A. Aharonian and C. W. Akerlof, Ann. Rev. Nucl. Part. Sci. 47 (1997) 273.

[4] R. A. Ong, Physics Reports 305 (1998) 93.

[5] D. Dumuro et al., *Čerenkov Low Energy Sampling & Timing Experiment, CELESTE experimental proposal*, LPNHE Ecole Polytechnique, Palaiseau (1996).

[6] R. A. Ong and C. E. Covault, *The STACEE project*, Proc. Towards a Major Atmospheric Cherenkov Detector V, Kruger Park, O. C. de Jager, ed., Potchefstrom University (1997), p. 247; astro-ph/9711301.

[7] T. C. Weekes et al., *Very Energetic Radiation Imaging Telescope Array System*, proposal, Smithsonian Astrophysical Observatory (1996).

[8] F. A. Aharonian et al., *High Energy Stereoscopic System*, letter of intent, Max Planck Institute for Nuclear Physics, Heidelberg (1997).

[9] O. Blanch et al., *The MAGIC telescope for gamma-ray astrophysics above 10–30 GeV*, letter of intent, Max Planck Institute for Physics, Munich (1998).

[10] D. Heck et al., *CORSIKA: A Monte Carlo code to simulate extensive air showers*, technical report FZKA 6019, Forschungszentrum Karlsruhe (1998).

[11] R. Nelson, technical report SLAC-Pub 265, Stanford Linear Accelerator Center (1985).

[12] F. X. Kneizys et al., *The MODTRAN 2/3 report and LOWTRAN 7 model*, Phillips Laboratory, Hanscom AFB, MA 01731, U.S.A. (1996).

[13] *U.S. Standard Atmosphere 1976*, U.S. Government Printing Office, Washington D.C. (1976).

[14] T. G. Kyle, *Atmospheric Transmission and Scattering*, Pergamon Press, Oxford (1991).

[15] F. A. Aharonian, W. Hofmann, A. K. Konopelko, H. J. Völk, Astropart. Phys. 6 (1997) 343.

[16] M. Hemberger and A. Konopelko, private communication (1997).

[17] E. Cuevas, Izana Global Atmospheric Watch (GAW) Observatory, private communication (1997).

[18] R. M. Baltrusaitis et al., Nucl. Instr. and Meth. A 240 (1985) 410.

[19] A. Karle et al., Astropart. Phys. 3 (1995) 321.

[20] M. Cassidy et al. (1997), Proc. 25^{th} Int. Cosmic Ray Conf., Durban, Vol. 5, p. 189; astro-ph/9707038.

[21] G. Pühlhofer et al., Astropart. Phys. 8 (1997) 101.